AD-A141 214 NUMERICAL SIMULATION OF THUNDERSTORM GUST FRONTS(U) AIR 1/1
FORCE GEOPHYSICS LAB HANSCOM AFB MA K L SEITTER
13 DEC 83 AFGL-TR-83-0329

UNCLASSIFIED F/G 4/2 NL

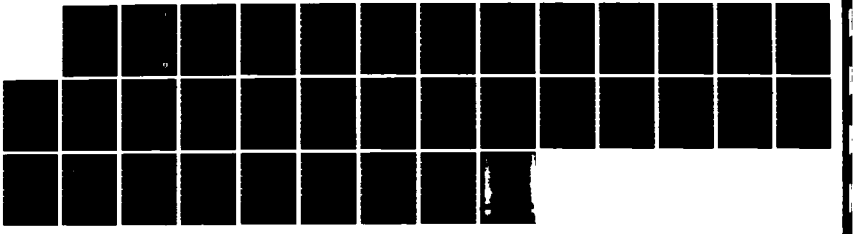

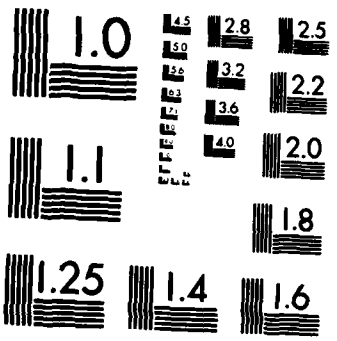

AFGL-TR-83-0329
ENVIRONMENTAL RESEARCH PAPERS, NO. 862

Numerical Simulation of Thunderstorm Gust Fronts

KEITH L. SEITTER

13 DECEMBER 1983

ATMOSPHERIC SCIENCES DIVISION PROJECT 6670
AIR FORCE GEOPHYSICS LABORATORY
HANSCOM AFB, MASSACHUSETTS 01731

AIR FORCE SYSTEMS COMMAND, USAF

This report has been reviewed by the ESD Public Affairs Office (PA) and is releasable to the National Technical Information Service (NTIS).

"This technical report has been reviewed and is approved for publication"

FOR THE COMMANDER

DONALD A. CHISHOLM, Chief
Atmospheric Prediction Branch

ROBERT A. McCLATCHEY, Director
Atmospheric Sciences Division

Qualified requestors may obtain additional copies from the Defense Technical Information Center. All others should apply to the National Technical Information Service.

If your address has changed, or if you wish to be removed from the mailing list, or if the addressee is no longer employed by your organization, please notify AFGL/DAA, Hanscom AFB, MA 01731. This will assist us in maintaining a current mailing list.

Do not return copies of this report unless contractual obligations or notices on a specific document requires that it be returned.

UNCLASSIFIED
SECURITY CLASSIFICATION OF THIS PAGE

REPORT DOCUMENTATION PAGE

1a. REPORT SECURITY CLASSIFICATION Unclassified	1b. RESTRICTIVE MARKINGS
2a. SECURITY CLASSIFICATION AUTHORITY	3. DISTRIBUTION/AVAILABILITY OF REPORT Approved for public release; distribution unlimited
2b. DECLASSIFICATION/DOWNGRADING SCHEDULE	
4. PERFORMING ORGANIZATION REPORT NUMBER(S) AFGL-TR-83-0329 ERP, No. 862	5. MONITORING ORGANIZATION REPORT NUMBER(S)
6a. NAME OF PERFORMING ORGANIZATION Air Force Geophysics Laboratory 6b. OFFICE SYMBOL (If applicable) LYP	7a. NAME OF MONITORING ORGANIZATION Air Force Geophysics Laboratory (LYP)
6c. ADDRESS (City, State and ZIP Code) Hanscom AFB Massachusetts 01731	7b. ADDRESS (City, State and ZIP Code) Hanscom AFB Massachusetts 01731
8a. NAME OF FUNDING/SPONSORING ORGANIZATION 8b. OFFICE SYMBOL (If applicable)	9. PROCUREMENT INSTRUMENT IDENTIFICATION NUMBER
8c. ADDRESS (City, State and ZIP Code)	10. SOURCE OF FUNDING NOS PROGRAM ELEMENT NO: 62101F; PROJECT NO.: 6670; TASK NO: 667010; WORK UNIT NO: 66701011
11. TITLE (Include Security Classification) NUMERICAL SIMULATION OF THUNDERSTORM GUST FRONTS	
12. PERSONAL AUTHOR(S) Keith L. Seitter*	
13a. TYPE OF REPORT Scientific 13b. TIME COVERED FROM 1 Oct 82 TO 30 Sep 83	14. DATE OF REPORT (Yr., Mo., Day) 1983 December 13 15. PAGE COUNT 34
16. SUPPLEMENTARY NOTATION *Present Affiliation: Department of Earth Sciences, University of Lowell Research performed while author participated in the Air Force Geophysics Scholar Program.	
17. COSATI CODES FIELD / GROUP / SUB GR	18. SUBJECT TERMS (Continue on reverse if necessary and identify by block number) Thunderstorm outflow, Gust front, Arc cloud, Density current

19. ABSTRACT (Continue on reverse if necessary and identify by block number)

The thunderstorm gust front is an important feature for both the maintenance and initiation of storms. Previous studies have shown that the thunderstorm outflow producing the gust front can be treated as an atmospheric density current to a good approximation. In this study, a new version of the density current speed equation, based on the surface pressure rise, is derived. This equation is shown to give much better results than other commonly used forms when applied to twenty previously reported gust front observations.

A two-dimensional numerical model is used to investigate the dynamics of atmospheric density currents. Simulations with this model show the effects of the environmental wind relative to the storm and the wind shear on the propagation of the gust front and the depth of the thunderstorm outflow. The results of these simulations are discussed in terms of the conditions necessary for the gust front to remain in a position that is beneficial for the maintenance of the storm.

20. DISTRIBUTION AVAILABILITY OF ABSTRACT UNCLASSIFIED UNLIMITED Σ SAME AS RPT Σ DTIC USERS Σ	21. ABSTRACT SECURITY CLASSIFICATION Unclassified
22a. NAME OF RESPONSIBLE INDIVIDUAL Donald A. Chisholm	22b. TELEPHONE NUMBER (Include Area Code) (617) 861-4729 22c. OFFICE SYMBOL AFGL/LYP

DD FORM 1473, 83 APR EDITION OF 1 JAN 73 IS OBSOLETE

UNCLASSIFIED
SECURITY CLASSIFICATION OF THIS PAGE

19. Abstract - Contd.

Moist processes are included in the model and simulations are made to investigate atmospheric density current propagation through a moist atmosphere. The lifting that occurs during gust front passage is calculated and it is found that even when this lifting is sufficient to bring moist parcels above their level of free convection; deep convection is prohibited by other aspects of the circulation. The generation of an arc cloud by the gust front is found to result in a less intense and slower gust front compared to an outflow that did not produce an arc cloud. This result is interpreted in terms of the gust front speed equation based on the surface pressure rise.

Preface

The author acknowledges the support of the Air Force Systems Command, the Air Force Office of Scientific Research and the Southeastern Center for Electrical Engineering Education during his appointment as an Air Force Geophysics Scholar. The staff of the Air Force Geophysics Laboratory (AFGL), especially the LYP Branch and the AFGL Computer Center, were very helpful throughout this project. Special thanks are due Dr. Kenneth Mitchell for many helpful discussions and Mr. Donald Chisholm for continual support. The author also thanks Ms. Betty Blanchard for typing this report.

All computations were performed on the AFGL CDC 6600 computer. Computer plots were made using the NCAR graphics software library translated for use on the AFGL system by P. Fougere.

A-1

Contents

Illustrations

Tables

Numerical Simulation of Thunderstorm Gust Fronts

1. INTRODUCTION

A relatively small but very important feature of thunderstorms is the gust front. The gust front is the leading edge of the cold downdraft air that spreads out upon reaching the ground. As shown in Figure 1, the gust front acts as a wedge that lifts low level air into the updraft of the thunderstorm. This maintains the thunderstorm by either supplying a continual inflow of potentially unstable air in the case of a supercell storm or initiating new updraft cells in the case of a multicell storm.[1] Gust fronts that have propagated well away from their parent thunderstorms can be responsible for the initiation of new thunderstorm activity, especially at the intersection of the gust front and some other air mass boundary or front.[2] Recent studies have indicated that the gust front may also play a role in tornado genesis.[3,4]

(Received for publication 29 Nov 1983)

1. Browning, K.A. (1977) The structure and mechanisms of hailstorms, Meteorol. Mono. 16(No. 38):1-43.

2. Purdom, J.F.W. (1976) Some uses of high-resolution GOES imagery in the mesoscale forecasting of convection and its behavior, Mon. Wea. Rev. 104:1474-1483.

3. Klemp, J.B., and Rotunno, R. (1983) A study of the tornadic region within a supercell thunderstorm, J. Atmos. Sci. 40:359-377.

4. Weaver, J.F., and Nelson, S.P. (1982) Multiscale aspects of thunderstorm gust fronts and their effects on subsequent storm development, Mon. Wea. Rev. 110:707-718.

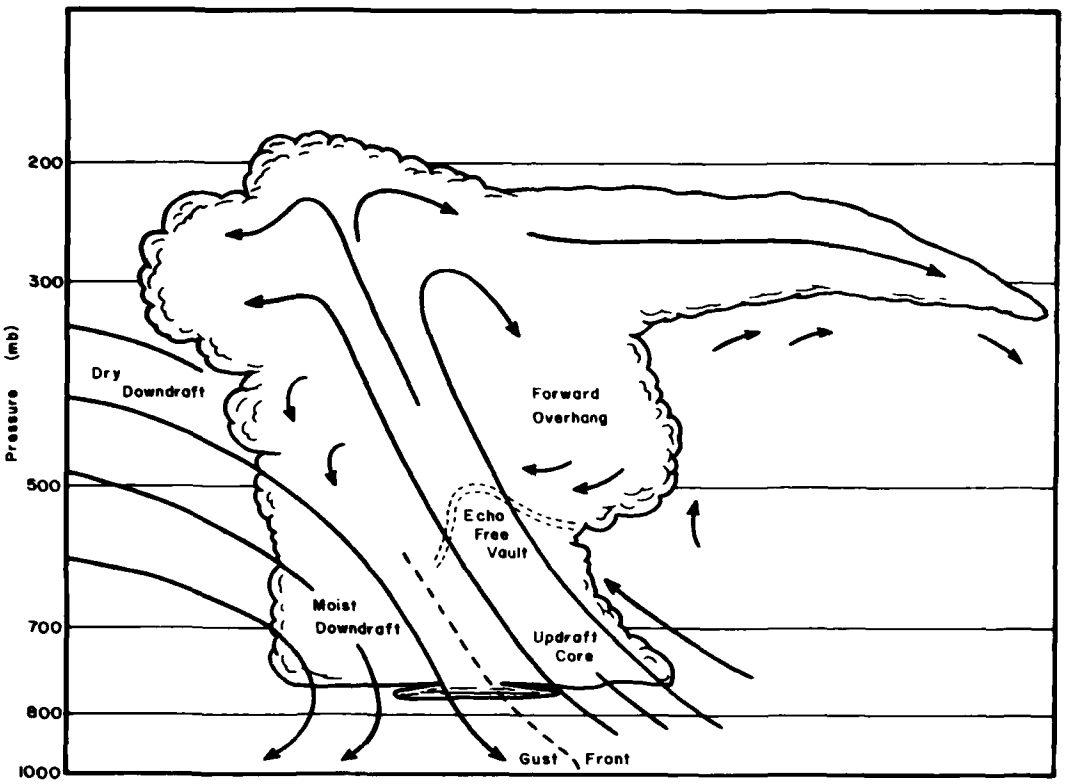

Figure 1. Cross-section Through a Supercell Type Thunderstorm[5]

Observational studies have shown that the cold air outflow from the thunderstorm can be treated as a density current.[6-8] A schematic of an atmospheric density current is shown in Figure 2. The current is characterized by an elevated head region, an overhanging nose, and a turbulent wake at the rear of the head. The arc cloud shown in Figure 2 is a commonly observed feature that is the result of moist boundary layer air being lifted above its level of condensation during the passage of the current.

---

5. Fritsch, J.M. (1975) Cumulus dynamics: Local compensating subsidence and its implications for cumulus parameterizations, Pure Appl. Geophys. 113:851-867.

6. Charba, J. (1974) Application of gravity current model to analysis of squall-line gust front, Mon. Wea. Rev. 102:140-156.

7. Goff, R.C. (1975) Thunderstorm outflow kinematics and dynamics, NOAA Tech. Memo, ERL NSSL-75, National Severe Storms Laboratory, Norman, Okla.

8. Wakimoto, R.M. (1982) The life cycle of thunderstorm gust fronts as viewed with Doppler radar and rawinsonde data, Mon. Wea. Rev. 110:1050-1082.

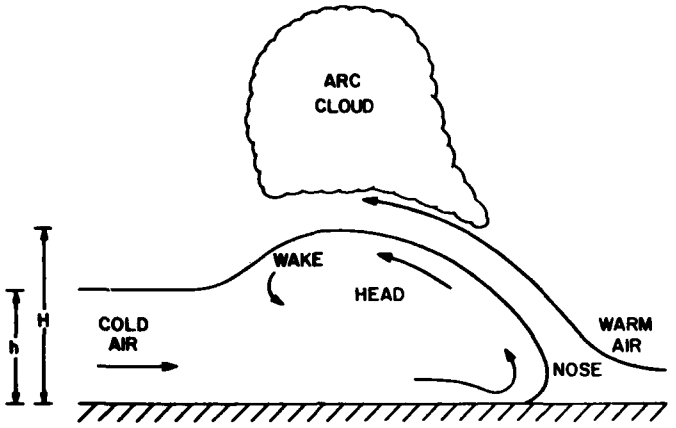

Figure 2. Schematic Representation of Atmospheric Density Current[7]

There have been many laboratory studies of density current motion[9] and several numerical studies.[10-12] While one of the laboratory studies dealt with the effect of ambient wind on the gust front motion,[9] none of these studies included the effect of the environmental shear commonly associated with severe storms or moist processes such as arc cloud formation. These studies also did not address the question of "gust front decoupling", the process by which the gust front separates from the parent storm and leads to the storms rapid decay.[8]

This research is meant to extend the work of the previous numerical and laboratory studies through the use of a numerical model. Specifically, the objectives were:

(a) Determine the effect of the ambient winds on gust front motion;

(b) Examine the effect of arc cloud generation on the gust front speed and intensity;

(c) Investigate the decoupling phenomena associated with gust fronts;

(d) Determine the profile of lifting that is associated with gust frontal passage;

9. Simpson, J.E., and Britter, R.E. (1980) A laboratory model of an atmospheric mesofront, Quart. J. Roy. Meteorol. Soc. 106:485-500.

10. Daly, B.J., and Pracht, W.E. (1968) Numerical study of density current surges, Phys. Fluids 10:15-30.

11. Mitchell, K.E., and Hovermale, J.B. (1977) A numerical investigation of the severe thunderstorm gust front, Mon. Wea. Rev. 105:657-675.

12. Thorpe, A.J., Miller, M.J., and Moncrieff, M.W. (1980) Dynamical two-dimensional downdraughts, Quart. J. Roy. Meteorol. Soc. 106:463-484.

(e) Show that the gust front can be accurately represented in a numerical model that uses the same resolution as current thunderstorm models.

One aspect of the study pertaining to objectives (a), (b), and (c) was the development of a more general gust-front speed equation than has been used in previous studies. This important result will be discussed in the following section.

2. THE GUST FRONT SPEED EQUATION

A major concern of many observational and laboratory studies of gust front and density current motion has been the determination of an equation relating the speed of the front to other measurable quantities.[6-9] Most of these studies used an equation of the form[13]

$$V = k^* \left[gh \frac{\Delta\rho}{\rho} \right]^{1/2} . \qquad (1)$$

In Eq. (1), V is the velocity of the front, g the acceleration of gravity, h the height of the denser fluid outflow, $\Delta\rho$ the difference in density between the current and the environment, and ρ the density of the environment. The constant, k^*, is the *internal Froude number*. *Benjamin*[13] *showed* that for two immiscible, inviscid fluids, $k^* = \sqrt{2}$.

In Eq. (1), the height, h, refers to the depth of the fluid behind the head. Since the ratio of the height of the head and the fluid depth behind the head is *nearly constant*,[13] a redefinition of the Froude number allows the use of the height of the head, H. If we assume that the density of air varies with temperature, $\rho = \rho_0 [1 + (T_{v0} - T_v)/T_v]$, where T_v is the virtual temperature and ρ_0 is the density at T_{v0}, then Eq. (1) may be rewritten for atmospheric density currents as

$$V = k \left[gH \frac{\Delta T_v}{T_v} \right]^{1/2} . \qquad (2)$$

In Eq. (2), ΔT_v is the difference in virtual temperature between the warm and cold air, T_v is the virtual temperature of the [illegible], and k is the redefined Froude number ($k = \sqrt{h/H}\, k^*$).

13. Benjamin, J.B. (1968) Gravity currents and related phenomena. J. Fluid Mech. 31:209-248.

Although theoretically the value of $k^* = \sqrt{2}$ and $k \approx 1.0$, the measured values of these quantities in the atmosphere and laboratory are substantially smaller. This is because the actual flows occur in fluids that have viscous and surface drag effects. These effects tend to reduce the speed from the theoretical limit, and this is incorporated into the value of the Froude number. There has been a fairly wide interval of k values obtained for atmospheric density currents and gust fronts ranging from $k = 0.70$ to $k = 1.08$[8].

The driving force of the density current is the pressure gradient force resulting from the increased hydrostatic pressure in the cold air. This is reflected in Eqs. (1) and (2), which may be rewritten in terms of the pressure.

Since the difference in surface hydrostatic pressure between the head region and the environment is $\Delta p = gH\Delta\rho$, Eq. (1) may be written (again with the redefined Froude number)

$$V = k\left[\frac{\Delta p}{\rho}\right]^{1/2} , \tag{3}$$

where Δp is the difference in surface hydrostatic pressure between the density current head and the environment.

For the constant density fluids assumed in the derivation of Eq. (1), all three of these equations will give identical results. However, for atmospheric density currents, the results given by these three equations will differ substantially. This is because Eqs. (1) and (2) deal only with the density differences over the height of the outflow, while Eq. (3) includes the integrated effect of the entire depth.

In applying Eq. (3) to observed atmospheric density currents, some assumptions must be made. The pressure difference, Δp, refers to the surface hydrostatic pressure in Eq. (3), but the measured pressure is the total surface pressure. Wakimoto[8] has shown, however, that the maximum surface pressure increase measured during the passage of the head is primarily hydrostatic and can therefore be used directly in Eq. (3). The numerical results of Mitchell and Hovermale[11] also indicate this. The density, ρ, in Eq. (3) is the average density of the warm air over the depth of the current, H. For ease of application, however, the surface density may be used in Eq. (3) with virtually no error.

It is common for gust fronts to propagate through environments that have an ambient wind. The component of the wind parallel to the gust front motion will affect its speed according to[9]

$$V = k\left[\frac{\Delta p}{\rho}\right]^{1/2} + 0.62\overline{U} \quad , \tag{4}$$

where $\overline{U}$ is the wind parallel to the gust front motion averaged over the depth of the head and positive in the direction of gust front motion.

In order to determine the value of k that applies to gust fronts when the pressure form of the equation is used, Eqs. (3) and (4) were applied to 20 observed gust fronts. These included the case studied by Charba,[6] the three cases of Wakimoto,[8] and the type I, II, and III cases of Goff.[7] The data on these cases included the recorded surface pressure rise, gust front speed, and ambient winds information. The surface value of the density in the warm air was used in all cases.

Figure 3 shows these observations plotted so that they should fall on a straight line with k as the slope. The best fit line through the origin gives k = 0.79. The correlation coefficient is 0.84. The numerical results of Mitchell and Hovermale[11] are also plotted in Figure 3, but were not used in determining the best fit line.

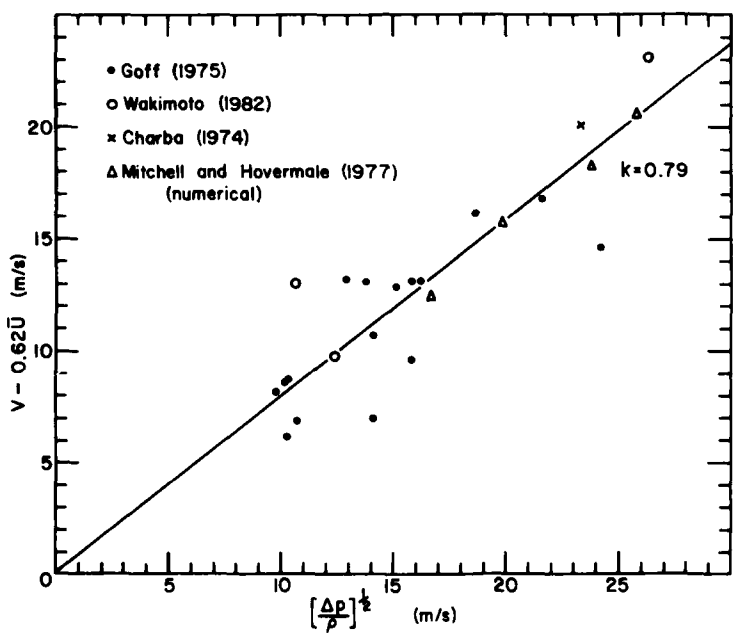

Figure 3. Observations of Gust Front Speed vs Surface Pressure Rise

The numerical results shown in Figure 3 fit the observational results very well. This shows that the numerical approach taken by Mitchell and Hovermale[11] captures the essential features of atmospheric density current motion, and justifies the extension of this approach taken in the present study.

3. THE NUMERICAL MODEL

3.1 The Equations

The model used to obtain the numerical results reported in this study is an improved version of the 2-D, Boussinesq, moist model developed by Seitter.[14] The domain is 40 km in the horizontal and 10 km in the vertical in the x-z plane, with a grid spacing of 500 m in both directions. The equations governing the vorticity, η, temperature, T, water vapor mixing ratio, q, and liquid water mixing ratio, m, are, respectively,

$$\frac{\partial \eta}{\partial t} + u\frac{\partial \eta}{\partial x} + w\frac{\partial \eta}{\partial z} = -g\frac{1}{\theta_0}\frac{\partial T_v}{\partial x} + g\frac{\partial m}{\partial x} + K\nabla^2\eta \quad , \tag{5}$$

$$\frac{\partial T}{\partial t} + u\frac{\partial T}{\partial x} + w\frac{\partial T}{\partial z} + w\Gamma_d = \frac{L}{c_p}G + K\nabla^2 T \quad , \tag{6}$$

$$\frac{\partial q}{\partial t} + u\frac{\partial q}{\partial x} + w\frac{\partial q}{\partial z} = -G + K\nabla^2 q \quad , \tag{7}$$

$$\frac{\partial m}{\partial t} + u\frac{\partial m}{\partial x} + w\frac{\partial m}{\partial z} + \frac{\partial}{\partial z}(V_t m) = G + K\nabla^2 m \quad . \tag{8}$$

The velocities, u and w, are written in terms of a streamfunction, ψ,

$$u = \frac{\partial \psi}{\partial z} \quad , \quad w = -\frac{\partial \psi}{\partial x} \quad , \tag{9}$$

$$\eta = \frac{\partial u}{\partial z} - \frac{\partial w}{\partial x} = \nabla^2\psi \quad . \tag{10}$$

In the above,

---

14. Seitter, K. L. (1982) The Dynamical Structure of Squall-line Type Thunderstorms, unpublished Ph. D. thesis, Dept. Geophys. Sci., Univ. of Chicago, 139 pp.

$T_v = (1 + 0.61q)T$ = virtual temperature,

θ_o = 300K,

Γ_d = 9.76°C/km = dry adiabatic lapse rate,

L = latent heat of condensation,

C_p = specific heat at constant pressure for dry air,

G = liquid water generation term,

V_t = precipitation fallspeed,

K = eddy viscosity.

The equations are finite differenced using the Arakawa Jacobian for the advective terms and the consistent nine-point finite difference form for the non-advective terms.[14] Time integration is performed using the Adams-Bashforth method with diffusion.[15] The Poisson equation for the streamfunction, Eq. (10), is solved after each time step by successive-over-relaxation. This equation is finite differenced using a fourth order differencing form to improve accuracy.

The condensation scheme that determines the value of G at each grid point is described in Seitter and Kuo.[15] Water condensed up to 1g/kg is assumed to be cloud water, and beyond this value it is assumed to fall as precipitation. The variable fallspeed formulation follows that of Liu and Orville,[16]

$$V_t = \begin{cases} 0 & \text{for } m \leq 1.0 \\ 5.32(m - 1.0)^{0.2} & \text{for } m > 1.0 \end{cases}, \qquad (11)$$

for m in g/kg and V in m/sec.

3.2 Surface Drag and Eddy Diffusion Formulation

The surface is treated as a "limited slip" surface following Mitchell and Hovermale.[11] In this formulation the boundary condition is applied as freeslip with a surface drag. Mitchell and Hovermale[11] applied this condition in a primitive equation model. Its application in a vorticity model is less obvious and requires careful consideration for consistency. The surface drag is applied as though it retarded only the surface velocity, which in turn modifies the

15. Seitter, K. L., and Kuo, H. -L. (1983) The dynamical structure of squall-line type thunderstorms, J. Atmos. Sci. 40:2831-2854.

16. Liu, J.Y., and Orville, H.D. (1969) Numerical modeling of precipitation and cloud shadow effects on mountain cumuli, J. Atmos. Sci. 26:1282-1298.

vorticity at the grid level just above the surface. The surface vorticity is held at zero as implied by a free-slip condition.

To evaluate the surface drag effect we must first calculate the surface velocity based on the interior flow. Using the definition of the vorticity and Eq. (9) we may write

$$\eta = \frac{\partial u}{\partial z} + \frac{\partial^2 \psi}{\partial x^2} \quad . \tag{12}$$

Then, using a centered difference for $\partial u/\partial z$, we can write the velocity at the surface (level 1), at the horizontal grid point i, in terms of the interior quantities

$$u_{i,1} = u_{i,3} - (2\Delta z) \left[\eta_{i,2} - \frac{\partial^2 \psi}{\partial x^2}\bigg|_{i,2} \right] \quad . \tag{13}$$

In general, the surface velocity calculated in this way will yield $u_{i,2} - u_{i,1} \neq 0$, that is, $\Delta u/\Delta z \neq 0$. This is, however, not a violation of the free-slip condition. The analytic free-slip condition is $\partial u/\partial z = 0$ at the surface. This leads to the specification of $\eta = 0$ on the lower boundary, since $w = \partial w/\partial x = 0$ there. The specification of $\eta = 0$ at the surface satisfies the analytic free-slip condition without reference to the velocity at level 2.

We now allow the surface velocity calculated in Eq. (13) to be retarded by a surface drag. The deceleration of $u_{i,1}$ by a bulk aerodynamic drag may be written[11]

$$\frac{\partial u_{i,1}}{\partial t}\bigg|_{\text{drag}} = - \frac{c_d |u_{i,1}|}{\Delta z} u_{i,1} \quad , \tag{14}$$

where c_d is the drag coefficient and Δz represents the depth of the layer over which the drag acts (one vertical grid spacing in this case).

The surface vorticity is unaffected by the deceleration of $u_{i,1}$, but the vorticity at level 2 must be modified. The rate of change of the vorticity at level 2 due to the drag is clearly

$$\frac{\partial \eta_{i,2}}{\partial t}\bigg|_{\text{drag}} = \frac{\partial}{\partial t}\left[\frac{\partial u}{\partial z}\bigg|_{\text{drag}} \right] = \frac{\partial}{\partial z}\left[\frac{\partial u}{\partial t}\bigg|_{\text{drag}} \right] \quad . \tag{15}$$

Since the drag is only applied at level 1, Eq. (15) reduces to

$$\left.\frac{\partial \eta_{i,2}}{\partial t}\right|_{\text{drag}} = \frac{c_d |u_{i,1}|}{2(\Delta z)^2}\, u_{i,1} \quad . \tag{16}$$

The surface drag effects are then included in the model by replacing the $K\nabla^2\eta$ term in Eq. (5) by the right side of Eq. (16) in the calculation of the time rate of change of vorticity at level 2. The diffusion term is omitted at this level because it would tend to diffuse zero vorticity from the surface into the interior of the domain, which is not desirable. If we set $c_d = 0$, we obtain a true free-slip boundary condition. In the model simulations, the drag coefficient was set at $c_d = 0.02$ following Mitchell and Hovermale.[11]

Note that the surface velocity calculated in Eq. (13) is a "true" surface velocity and not a nonphysical numerical quantity. Therefore, this velocity can be used to advect surface values of the trace variables with physical justification. This formulation can easily be generalized to an anelastic model.

The diffusion of quantities by turbulent eddies is treated with a Fickian diffusion term using a nonlinear eddy viscosity, K. We let

$$K = K_o + K^* |\nabla^2 \eta| \quad , \tag{17}$$

where K_o and K* are constants. K_o is a constant eddy coefficient that is required to stabilize the Adams-Bashforth method. A value of at least 150 m^2/sec is required to allow a relatively large timestep (10 sec), so that the model can be economically used for a large number of simulations. Two forms of K were used in the simulations presented here. These will be discussed in connection with the two cold air source types presented later in this section.

3.3 Other Boundary Conditions

Lateral boundary conditions are always an important concern in limited area modeling. This model uses a 2-D radiation condition on the vorticity

$$\frac{\partial \eta_b}{\partial t} + C_x \frac{\partial \eta_b}{\partial x} + C_z \frac{\partial \eta_b}{\partial z} = 0 \quad , \tag{18}$$

where η_b is the value of the vorticity at the boundary. In Eq. (18), C_x and C_z represent the speed of an outgoing wavelike disturbance perpendicular to and parallel to the boundary, respectively, and are calculated from the interior solution. The numerical implementation of this condition is outlined in Seitter and Kuo.[15] The other variables satisfy

$$\frac{\partial \phi}{\partial t} = 0 \qquad \text{u into domain} \tag{19a}$$

$$\frac{\partial \phi}{\partial t} + u \frac{\partial \phi}{\partial x} = 0 \qquad \text{u out of domain} \quad , \tag{19b}$$

where $\phi = T, q, m$, and $u = \partial \psi / \partial z$ at the lateral boundary. Neumann conditions, $\partial \psi / \partial x = 0$, are specified for the streamfunction.

The top and bottom boundaries are taken as rigid plates, so the streamfunction is constant on these boundaries. The vorticity is set equal to zero on the top boundary. The other variables are held fixed on the top boundary with the temperature and water vapor mixing ratio held equal to the environmental values and the liquid water specified as zero. On the bottom boundary, rain is permitted to fall "through" the surface by specifying

$$\frac{\partial m}{\partial t} + \frac{\partial}{\partial z} (V_t m) = 0 \quad . \tag{20}$$

The bottom is allowed to cool by evaporation if rain is present by specifying

$$\frac{\partial T}{\partial t} + U_o \frac{\partial T}{\partial x} = \frac{L}{C_p} G \quad , \tag{21}$$

$$\frac{\partial q}{\partial t} + U_o \frac{\partial q}{\partial x} = - G \quad , \tag{22}$$

where

$$G = \begin{cases} -E & m > 0, \ RH < 90\% \\ 0 & \text{otherwise} \end{cases} \quad , \tag{23}$$

where $E = 4.0 \times 10^{-6} \text{sec}^{-1}$ is the constant evaporation rate used in the model. Equations (21) and (22) allow rain to evaporate up to a relative humidity of 90 percent, and for the surface values of T and q to be advected by the surface wind. The surface wind, U_o, is given by Eq. (13).

3.4 Cold Air Source

The density current is initiated by a cold air source located near the left boundary. Two types of cold air sources were used. The first, referred to as M-type, is a fixed temperature source based on the work of Mitchell and Hovermale.[11] For this source, the temperature in the source region is given initially by

$$T = T_{env.} - \Delta T[\cos(2\pi/L\,(z - z_0))\,\cos(2\pi/L\,(x - x_0))] \quad , \tag{24}$$

for $|z - z_0| \leq L/4$ and $|x - x_0| \leq L/4$, where L = 12 km. $T_{env.}$ is the temperature of the undisturbed environment at that height. Once the integration is begun only the top half of this region is maintained at this temperature. While this source has the desirable property of providing cold air at a fixed temperature, it requires a large eddy viscosity, K = 900 m^2/sec, to suppress noise that is generated near the source. In the eddy viscosity formulation, K_o = 900 m^2/sec and K* = 0, so for the simulations using the M-type source, the formulation reduces to a constant eddy viscosity. The model was stable for smaller values of K, but the value used confined the noise to the immediate region of the cold air source.

A second type of cold air generator used is based on the work of Thorpe et al[12] and is referred to as the Q-type source. This source applies a constant cooling rate of the form

$$\frac{\partial T}{\partial t} = -Q[\cos(2\pi/L\,(z - z_0))\,\cos(2\pi/L\,(x - x_0))] \quad , \tag{25}$$

for $|z - z_0| \leq L/4$ and $|x - x_0| \leq L/4$. Q is the cooling rate in the generator region. This source produces a smoother temperature field in the source region and allows the use of the full nonlinear eddy viscosity formulation. In the Q-type simulations, K_o = 150 m^2/sec and K* = 1.2 $\times 10^{10}$ m^4. With these values of K_o and K*, K reached maximum values of about 600 m^2/sec in the turbulent head region while the domain average never exceeded 200 m^2/sec. The density currents produced using the Q-type source in the present study were not as steady as those obtained with the M-type source because the flux of cold air tended to pulsate.

4. M-TYPE SOURCE RESULTS

4.1 Stationary Source

This section will describe the results obtained with the model using the M-type cold air source and a dry atmosphere with no environmental winds. In all simulations, the atmosphere had a constant lapse rate and a surface temperature of 295 K. The results for the M-type simulations are summarized in Table 1. The quantities listed in this table were measured in the numerical results after the density current became steady. Steadiness was generally reached by the time the leading edge of the current was 10 km from the source region, which usually occurred by 15 minutes into the integration.

Figure 4a shows the temperature distribution for one of these simulations, case MD2, after 20 min of integration. Note the accurate representation of the head region compared to Figure 2. No nose is evident in this figure, but observational and laboratory studies indicate that the nose would be below 500 m and thus not resolvable in the model. The outflow depth is quite large in this simulation because of the small static stability ($\partial\theta/\partial z$ = 0.2°C/km), but is almost exactly that predicted by Mitchell[17] for this stability.

The streamfunction for case MD2 is analyzed in Figure 4b. The symmetry of the streamlines around the source region shows the ability of the 2-D lateral boundary condition to accurately allow inflow and outflow through the boundary. A packing of the streamlines is evident at the surface near the frontal boundary of the outflow. The high wind gust just behind the front associated with this packing is a commonly observed feature during gust frontal passage[6,7] and has been shown to be a result of the surface drag.[11]

A more realistic depth is obtained for the outflow if a larger and more realistic environmental stability is used. The result of one of these simulations, case MD9, is shown in Figure 5. In this figure, the potential temperature is analyzed instead of the temperature. In this representation, the outflow is delineated by the 295 K isentrope.

4.2 Sensitivity to Model Parameters

The eddy viscosity and surface drag coefficient are two parameters that are difficult to choose on purely physical grounds. Therefore, three sensitivity simulations were carried out which were identical to MD2 except for changes in one of these parameters. The results of these simulations are given in Table 2.

17. Mitchell, K.E. (1975) A Numerical Investigation of Severe Thunderstorm Gust Fronts, unpublished M.S. thesis, the Pennsylvania State University, 104 pp. (Also available from NTIS, No. N76-17737/7GI)

Table 1. Results of M-type Simulations

Case	Source ΔT (^{o}C)	Stability $(\partial\theta/\partial z)$ ($^{o}C/km$)	Source Velocity (m/sec)	Ambient Shear ($\times 10^{-3} s^{-1}$)	ΔT at Head (^{o}C)	H (km)	$\overline{U}$ (m/s)	V (m/s)	Updraft at Front (m/sec)	Δp at Head (Pa)	k
MD1	4.0	0.2	0	0	2.0	3.2	0	11.9	5.7	357.0	0.70
MD2	8.0	0.2	0	0	4.7	3.3	0	17.3	10.1	706.6	0.72
MD3	8.0	0.2	5.0	0	5.0	3.7	0	18.3	11.4	835.7	0.70
MD4	8.0	0.2	10.0	0	4.8	4.4	0	18.8	12.0	991.0	0.66
MD5	8.0	0.2	0	0	4.5	4.2	-10.0	11.1	10.5	879.8	0.73
MD6	8.0	0.2	10.0	2.0	4.1	4.2	4.2	21.8	13.0	815.0	0.71
MD7	8.0	0.2	20.0	4.0	6.3	4.1	8.2	28.1	18.2	1020.7	0.73
MD8	4.0	1.46	0	0	1.7	1.3	0	11.8	1.7	369.6	0.68
MD9	8.0	1.46	0	0	3.9	2.1	0	17.7	5.0	877.0	0.70
MD10	8.0	1.46	10.0	0	4.3	2.4	0	19.6	6.1	1022.4	0.68
MM1	4.0	1.46	0	0	2.0	1.8	0	11.0	2.1	299.2	0.71
MM2	8.0	1.46	0	0	4.7	2.1	0	15.3	4.8	610.4	0.69
										Ave.	0.70

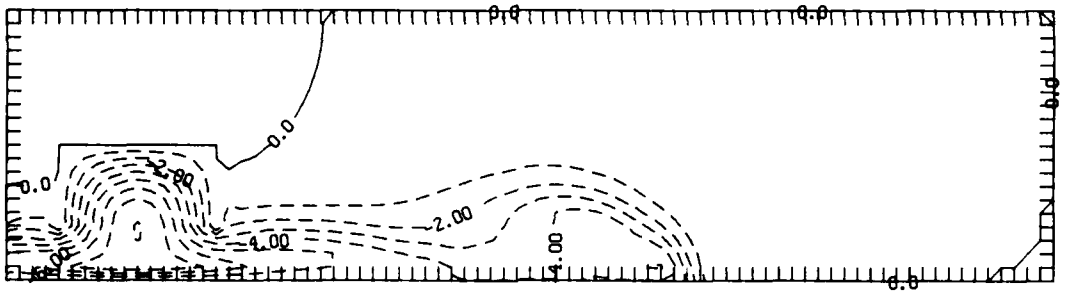

Figure 4a. Temperature Distribution for Case MD2 at 20 min. Cold source region is at the left and the density current is propagating from left to right. Contours give temperature departures in ^{o}C and tick marks are at 500-m intervals

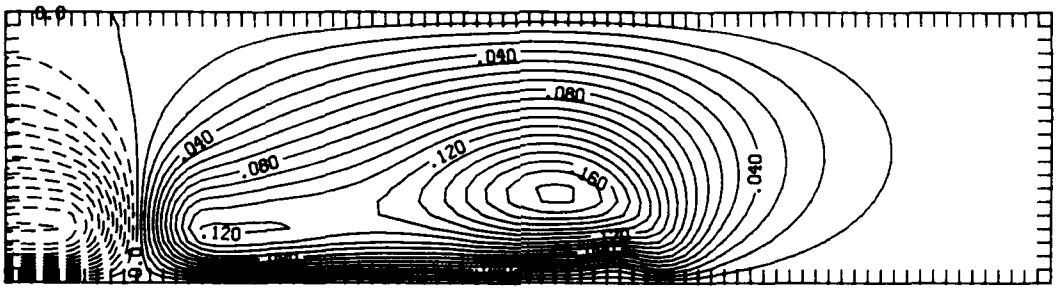

Figure 4b. Streamfunction Analysis for Case MD2 at 20 min. Contours are labeled in nondimensional units

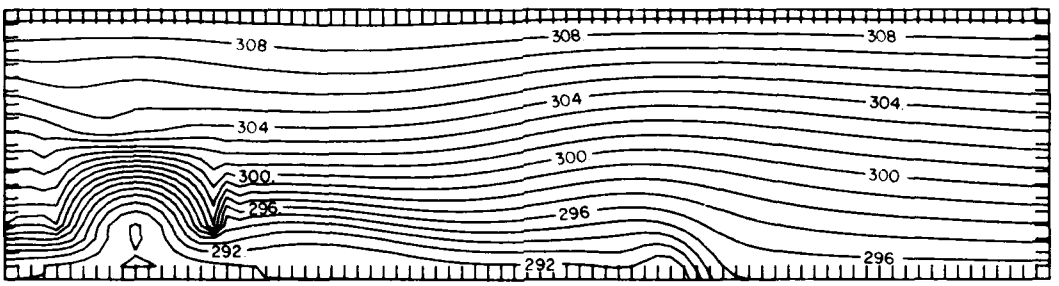

Figure 5. Potential Temperature Distribution for Case MD9 at 20 min

Table 2. Sensitivity Experiment Results

Case	ΔT at Front (°C)	H at Head (km)	V (m/sec)	Δp at Head (Pa)	k	Parameter Modification
MD2	4.7	3.3	17.3	706.6	0.72	none
MD2A	4.7	3.3	18.4	666.9	0.78	$K = 450\ m^2/sec$
MD2B	4.4	3.3	19.3	692.9	0.81	$C_d = 0.0$
MD2C	4.5	3.2	16.3	691.1	0.69	$C_d = 0.04$

In case MD2A, the eddy viscosity was halved to a value of $K = 450\ m^2/sec$. The resulting density current was nearly identical to MD2, but propagated a little over 1 m/sec faster due to the decreased viscous drag. This resulted in an increase in the Froude number of about 8 percent. A detailed analysis of the effect of viscosity on the speed of the gust front was carried out by Daly and Pracht.[10] Although exact comparison with their results is not possible, they are consistent with the results found here.

For cases MD2B and MD2C, the surface drag was set at $c_d = 0$ and $c_d = 0.04$, respectively, instead of the $c_d = 0.02$ used in the rest of the simulations. As would be expected, the gust front speed was inversely related to the surface drag while the current shape and surface hydrostatic pressure rise were relatively unaffected. The percentage change in the frontal speed for these simulations was almost identical to the corresponding experiments in the more complete sensitivity tests performed by Mitchell and Hovermale.[11]

4.3 Moving Source

As the thunderstorm propagates, the downdraft represents a moving cold air source, so it is of interest to consider the effect that movement of the source has on the resulting density current. This extension to previous studies is made possible by the excellent lateral boundary conditions used in the current model. Numerically, it is much easier to subtract a velocity from the domain than to advect the source, so this is the approach taken. Note that the velocity must also be subtracted in the surface drag formulation so that the proper drag is applied.

An interesting result pertains to the time at which the source is set in motion. If the density current is allowed to propagate on the order of 15 km away from the source while the source is stationary, and then the source is set in motion at a speed less than or equal to the dens current speed, the resulting

density current is indistinguishable from one in which the source is stationary for the entire integration. In fact, if the source is set in motion at the speed of the current, the source/current system remains nearly steady with the current showing virtually no propagation relative to the source. In this situation we may say that the gust front is "decoupled" from the source in the sense that its speed is determined by its local characteristics.

If the source is moving at the start of the integration, the resulting density current is modified relative to that given by a stationary source. This is illustrated by comparing the results in Table 1 of the moving source cases (MD3, MD4, and MD10) with the corresponding stationary source cases (MD2 or MD9). In the moving source simulations, cold air is "piled up" near the source during the early stages of the integration before the current propagates a sufficient distance to be decoupled. This greater depth results in a higher hydrostatic pressure and thus a greater speed.

Figure 6 shows the density current that results from having the source move at 10 m/sec. This simulation, case MD4, was identical to MD2 except for the movement of the source. Note that Figure 6 is in the source relative frame, so that the front is moving faster than in case MD2 even though it has traveled less far in the domain by the 20-min point. The piling up of cold air is quite evident when this figure is compared with Figure 4a.

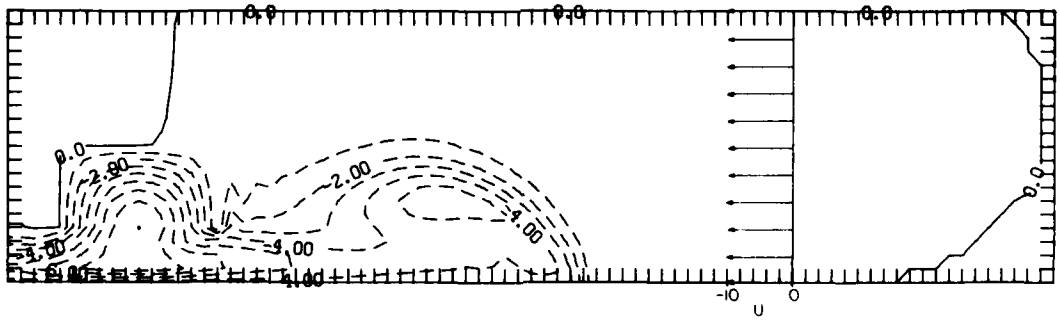

Figure 6. Temperature Distribution for Case MD4 at 20 min. Source relative winds are plotted in m/sec

Since most severe thunderstorms develop in environments exhibiting vertical shear, constant vertical shear was included in simulations MD6 and MD7. The results of case MD6 after 20 min of integration are shown in Figure 7a. For this simulation the source moved at 10 m/sec and the environmental shear was $2 \times 10^{-3} sec^{-1}$. Because of the shear, the frontal boundary tends to be retarded

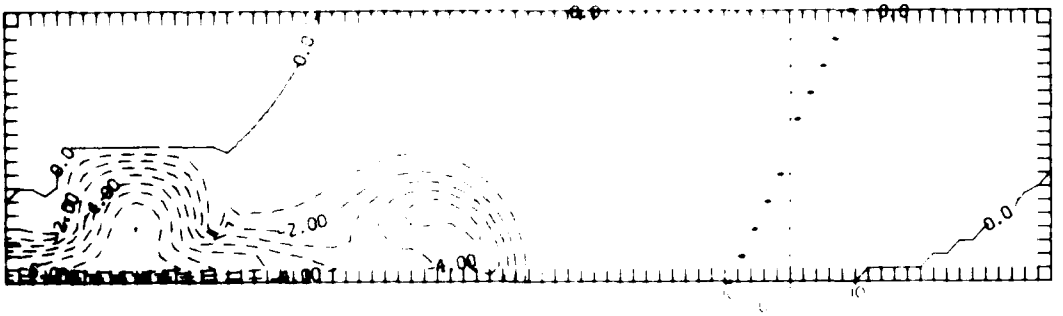

Figure 7a. Temperature Distribution for Case MD6 at 20 min. Source relative winds are plotted in m/sec

more near the surface than above so the frontal boundary becomes more vertical. The current shapes in these simulations were very similar to the gust front observed by Charba.[6] The streamfunction for this case, analyzed relative to the source, is shown in Figure 7b. This figure shows how the gust front can act to cut off the low level inflow to the updraft if it propagates well ahead of the storm.

A simulation was also run with a source speed of 20 m/sec and a shear of $4 \times 10^{-3} sec^{-1}$. The results of this case, MD7, are given in Table 1. Since the source was moving very fast in this case, the density current did not begin propagating away from the source until it had achieved a sufficient temperature difference and depth for its density current speed to be greater than the source speed. Its close proximity to the source for a considerable length of time resulted in substantially lower temperatures in the head.

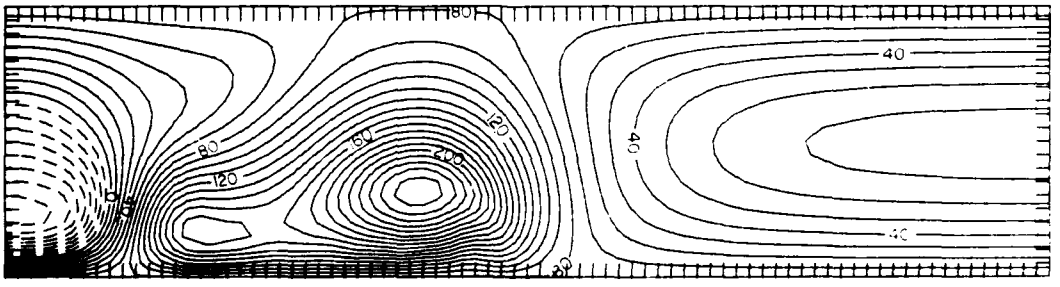

Figure 7b. Streamfunction Analysis for Case MD6 at 20 min

The density currents in the simulations with shear are moving through an environment with an effective ambient wind equal to the average winds over the depth of the current. Therefore, Eq. (4) must be used to calculate the appropriate value of k. For cases MD6 and MD7, and for case MD5, which had a stationary source but constant ambient wind, it was found that the best agreement was obtained when 0.85 $\overline{U}$ was used in Eq. (4) rather than 0.62 $\overline{U}$. Therefore, the k values shown in Table 1 use this form. The other values of k shown in Table 1 were calculated using Eq. (3). The average k value for the M-type simulations was k = 0.70.

4.4 Moist Simulations With M-type Source

To study the effect arc cloud generation has on gust front motion, two simulations were carried out in a moist atmosphere. The environment had a relative humidity of 50 percent in the lowest 1.5 km and 20 percent above 3 km with a linear transition layer between.

The results of these two simulations, cases MM1 and MM2, are also shown in Table 1. The high diffusion required for the M-type source appeared to significantly affect the arc cloud liquid-water distribution. The Q-type source allows a much smaller diffusion, which is less likely to adversely affect the liquid water distribution. Therefore, although the results shown in Table 1 are consistent with the Q-type simulations, the effect of the arc cloud on the gust front motion will be discussed in terms of the Q-type source results.

5. Q-TYPE SOURCE RESULTS

5.1 Dry Results

The results of the Q-type simulations are given in Table 3. The dry simulations were carried out for a stationary source using several source strengths and stabilities. The dry simulation results using the Q-type source were very similar to those of the M-type source. The average value of the Froude number was k = 0.75, and is somewhat larger than the M-type value. This is probably a reflection of the smaller eddy viscosity used in the Q-type simulations. Although the flux of cold air tended to pulsate in the Q-type simulations, the flow in the vicinity of the density current head became fairly steady after 10 to 15 minutes of integration.

Figure 8 shows the potential temperature field for case QD5 at 20 min. The density current produced in this simulation is very similar to the one shown in Figure 5, which was produced by the M-type source. The smoother nature of

Table 3. Results of Q-type Simulations

Case	Source Cooling Rate (°C/min)	Stability ($\partial\theta/\partial z$) (°C/km)	Low Level Humidity (%)	ΔT at Head (°C)	H (km)	V (m/sec)	Updraft at Front (m/sec)	k Eq. (2)	Δp at Head (Pa)	k Eq. (3)
QD1	1.0	0.2	dry	3.3	2.4	13.0	6.4	0.80	343	0.77
QD2	2.0	0.8	dry	5.3	1.9	16.4	6.8	0.91	585	0.75
QD3	1.0	1.46	dry	3.0	1.4	11.8	2.6	0.99	325	0.73
QD4	2.0	1.46	dry	4.1	1.7	15.3	4.1	1.01	530	0.74
QD5	3.0	1.46	dry	5.8	1.9	18.1	6.2	0.95	755	0.73
QM1	2.0	1.46	50	4.3	1.6	14.4	4.6	0.96	476	0.73
QM2	2.0	1.46	60	4.6	1.7	13.0	3.8	0.81	364	0.75
QM3	3.0	1.46	60	6.2	1.8	15.0	4.8	0.80	502	0.74
QM4	2.0	1.46	70	4.8	1.7	11.0	3.9	0.68	246	0.78
									Ave.	0.75

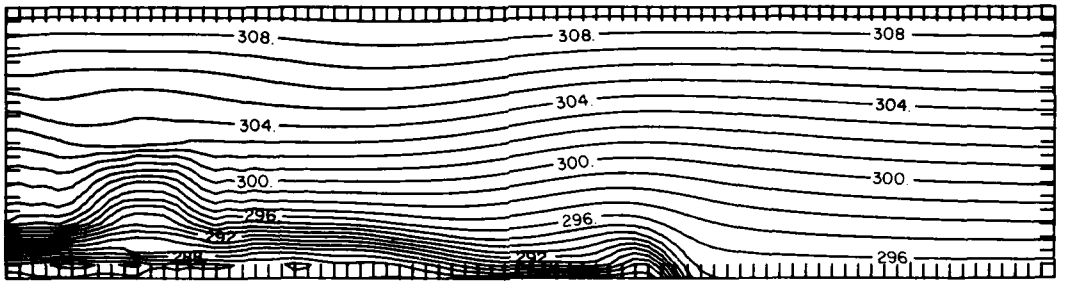

Figure 8. Potential Temperature Field for Case QD5 at 20 min

the source region, despite the smaller diffusion used in the Q-type simulations, is evident in a comparison of these two figures. The height of the head was somewhat less in the Q-type simulations than in the M-type for a given temperature difference and stability. The reason for this result is not clear.

The lifting experienced during gust frontal passage was determined by computing the trajectories of parcels originally in the calm air ahead of the front using the method of Schlesinger.[18] The lifting profile for this case is shown in Figure 9. It was found that even though the density current is a shallow phenomenon, lifting is experienced by parcels throughout the depth of the troposphere with the amount of lifting decreasing linearly with height. This result is of direct relevance to the work of Matthews[19] who was forced to compare several lifting profiles in his 1-D model simulations because of lack of guidance in this aspect of gust front passage.

Given the stability of the environment, $\partial\theta/\partial z = 1.46^{o}C/km$, the lifting of air by the head of the current results in a cooling of the column above the head, which contributes to the surface hydrostatic pressure. Therefore, Eq. (2) gives a different result than Eq. (3) since it considers only the temperature difference between the low level environment and the current itself. For a nearly neutral environment, as in case QD1 where $\partial\theta/\partial z = 0.2^{o}C/km$, the lifting does not result in much cooling, thus the values of k computed using Eqs. (2) and (3) are nearly the same. Table 3 lists the values of k computed using both Eqs. (2) and (3). It is clear that the simulated density currents satisfy the density current speed equation very well when the pressure form Eq. (3) is used. The average value of k computed using Eq. (3) is also very nearly the same as that given by observations of gust fronts.

18. Schlesinger, R.E. (1973) A numerical model of deep moist convection: Part A prototype experiment and variations upon it, J. Atmos. Sci. 30:1374-1391.

19. Matthews, D.A. (1981) Observations of a cloud arc triggered by thunderstorm outflow, Mon. Wea. Rev. 109:2140-2157.

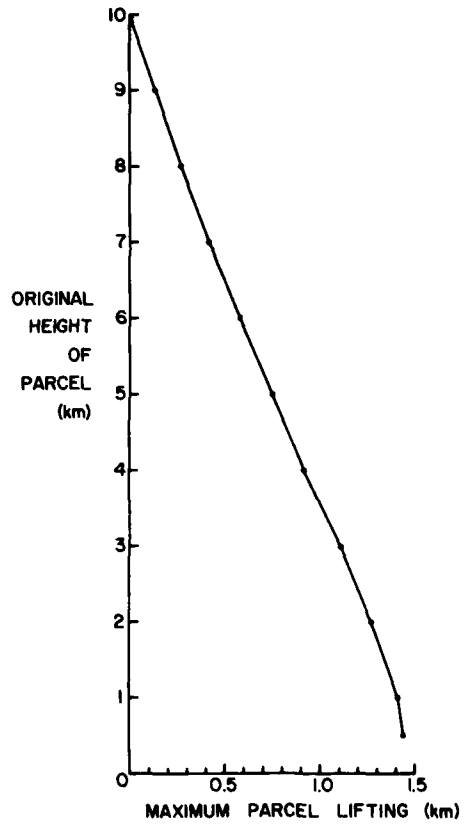

Figure 9. Lifting Experienced by Parcels During Gust Front Passage for Case QD5

5.2 Moist Results

The results for simulations in a moist atmosphere, with low level humidities varying from 50 percent to 70 percent, are given in Table 3. The potential temperature distribution for one of these simulations, case QM2 at 25 min is shown in Figure 10a. Figure 10b shows the arc cloud location in the liquid water distribution superimposed on the potential temperature field. For clarity, only the center 20 km of the 40-km domain is shown. The potential temperature distribution does not show the typical head structure associated with density currents. The existence of the head is evident, however, in the raised isentropes at upper levels. The cloud is suppressed behind the head by the subsidence existing there, but not completely dissipated. All of the moist simulations

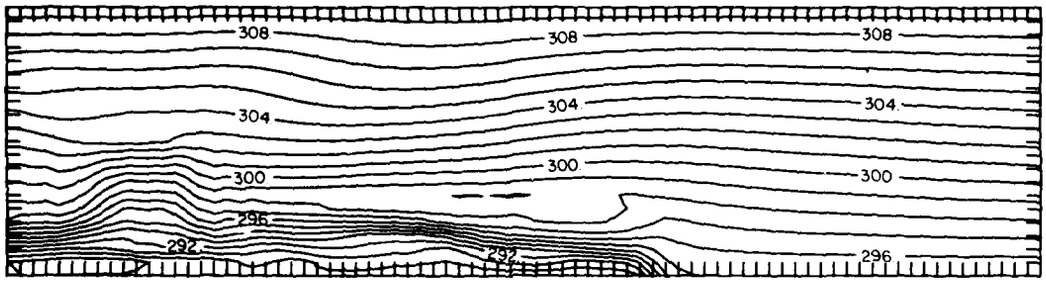

Figure 10a. Potential Temperature Distribution for Case QM2 at 25 min

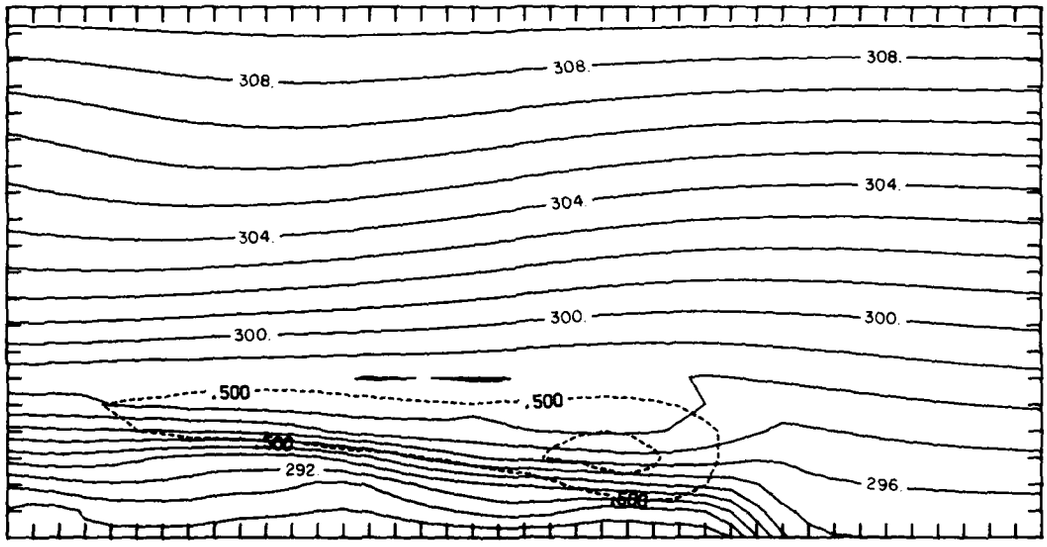

Figure 10b. Liquid Water Field for Case QM2 at 25 min Superimposed on the Potential Temperature Field. Liquid water contour interval is 0.5 g/kg. Only the center 20 km of the 40 km domain is shown

exhibited are cloud development except QM1, but only QM4 had precipitation reach the ground under the arc cloud.

The arc cloud is produced by the low level air being lifted by the current above its condensation level. The release of latent heat associated with this condensation produces a warm pocket at the top of the head, which results in the isentropic structure shown in Figure 10b. The air over the head has, in fact, been raised above its level of free convection and is warmer than the environment. However, deep convection does not develop even in this conditionally

very unstable atmosphere. It is felt that the convection is suppressed for two reasons. First, the air lifted by the current is quickly raised above the head and then, as the head passes, it subsides in the wake region. An individual parcel is only above its level of free convection for a short period of time before being forced downward. Secondly, the frontal boundary above the head is a region of strong shear, which will inhibit convection. The lack of deep convection initiation is an interesting result. Satellite observations of gust fronts have shown them to propagate large distances producing shallow cumulus, but initiate deep convection only after they intersect with another outflow boundary that provides additional lifting.[3]

The production of the warm pocket above the head has a pronounced effect on the speed of the gust front. This warm air decreases the surface hydrostatic pressure under the head (although the weight of the liquid water provides a slight increase) and therefore reduces the pressure gradient force driving the current. Thus, the moist current propagates at a slower speed than would a dry current of the same depth and temperature difference. This fact is evident in Table 3 through the comparison of the dry and moist simulation results. For instance, comparing QD4 and QM2, we can see that although both are the same depth and QM2 has a larger temperature difference than QD4, QM2 propagates slower than QD4. This is in direct conflict with Eq. (2), but is easily explained through Eq. (3). The warm pocket above the head in QM2 results in a smaller surface pressure difference, and therefore a slower speed of propagation.

Table 3 also lists the calculated updraft velocity at the front. These values compare very well with those obtained by Mitchell and Hovermale.[11] This upward motion is primarily accomplished by mechanical lifting even in the moist cases. Because of this, for a given stability, the updraft speed is determined almost entirely by the speed and depth of the density current. The upward motion is suppressed in the more stable environments, as would be expected. If the release of latent heat is sufficient, the updraft in the moist cases will be augmented by the buoyancy of the parcels. This is evident in a comparison of cases QM2 and QM4.

6. CONCLUSIONS

This report has presented a somewhat different version of the gust front speed equation based on the surface pressure difference between the density current head and the environment. It was shown through the use of numerical simulations that this form of the equation gives much more consistent results than the other commonly used forms. It is also easier to apply to observations since only

the surface values of the thermodynamic variables are needed. Twenty observed gust front cases were re-analyzed in terms of this equation and the appropriate internal Froude number was found to be k = 0.79.

This study also showed that accurate representation of the thunderstorm outflow and gust front can occur in a model with relatively coarse resolution in the vertical. This is an important consideration in numerical thunderstorm models, which have a similar resolution but depend on gust front effects for maintenance of the storm. It should, however, be noted that proper treatment of the surface drag was found to be essential, especially at this relatively coarse resolution.

Simulations with a moving cold air source shed light on the gust-front decoupling process. Once the gust front has propagated a sufficient distance from its source region, its speed is determined by its local characteristics. However, the source region can have a great deal of influence on the outflow if the ambient wind and source speed act to keep the gust front close to the source. This indicates that modulations in the thunderstorm strength and speed may act to retain the gust front in a position which is beneficial to the storm. Any possible feedback mechanism that could control the modulations must keep the gust front from propagating beyond its decoupling distance in order to produce a long-lived storm.

The warm pocket produced above the head during arc cloud formation tends to result in a slower gust front than a corresponding outflow, which did not produce an arc cloud. This decrease in speed is a result of the decreased surface hydrostatic pressure rise. Deep convection is not initiated by the gust front, even when parcels are lifted above their level of free convection during gust front passage, indicating that an additional trigger mechanism may be necessary.

This study has produced some very interesting results concerning the effects of ambient winds and moisture on density current motion. Many of these results have direct bearing on the speed, depth, and intensity of thunderstorm outflows and their associated gust fronts. Further work is required, however, to truly quantify these effects. The result that the lifting is experienced throughout the depth of the troposphere indicates that results from an anelastic model should be included in this study. Further, a more complete series of moving source and sheared environment studies should be carried out in a more stable environment, where the density current would have a more realistic depth. This shallower depth would require a higher resolution in the vertical (say, 200 m) in order to allow the proper interaction of the current with the shear. The effects of the shear may be considerably reduced for shallow currents.

References

1. Browning, K.A. (1977) The structure and mechanisms of hailstorms, Meteorol. Mono. 16(No. 38):1-43.
2. Purdom, J.F.W. (1976) Some uses of high-resolution GOES imagery in the mesoscale forecasting of convection and its behavior, Mon. Wea. Rev. 104:1474-1483.
3. Klemp, J.B., and Rotunno, R. (1983) A study of the tornadic region within a supercell thunderstorm, J. Atmos. Sci. 40:359-377.
4. Weaver, J.F., and Nelson, S.P. (1982) Multiscale aspects of thunderstorm gust fronts and their effects on subsequent storm development, Mon. Wea. Rev. 110:707-718.
5. Fritsch, J.M. (1975) Cumulus dynamics: Local compensating subsidence and its implications for cumulus parameterizations, Pure Appl. Geophys. 113:851-867.
6. Charba, J. (1974) Application of gravity current model to analysis of squall-line gust front, Mon. Wea. Rev. 102:140-156.
7. Goff, R.C. (1975) Thunderstorm outflow kinematics and dynamics, NOAA Tech. Memo, ERL NSSL-75, National Severe Storms Laboratory, Norman, Okla.
8. Wakimoto, R.M. (1982) The life cycle of thunderstorm gust fronts as viewed with Doppler radar and rawinsonde data, Mon. Wea. Rev. 110:1050-1082.
9. Simpson, J.E., and Britter, R.E. (1980) A laboratory model of an atmospheric mesofront, Quart. J. Roy. Meteorol. Soc. 106:485-500.
10. Daly, B.J., and Pracht, W.E. (1968) Numerical study of density current surges, Phys. Fluids 10:15-30.
11. Mitchell, K.E., and Hovermale, J.B. (1977) A numerical investigation of the severe thunderstorm gust front, Mon. Wea. Rev. 105:657-675.
12. Thorpe, A.J., Miller, M.J., and Moncrieff, M.W. (1980) Dynamical two-dimensional downdraughts, Quart. J. Roy. Meteorol. Soc. 106:463-484.

13. Benjamin, J. B. (1968) Gravity current and related phenomena, J. Fluid Mech. 31:209-248.

14. Seitter, K. L. (1982) The Dynamical Structure of Squall-line Type Thunderstorms, unpublished Ph.D. thesis, Dept. Geophys. Sci., Univ. of Chicago, 139 pp.

15. Seitter, K. L., and Kuo, H. -L. (1983) The dynamical structure of squall-line type thunderstorms, J. Atmos. Sci. 40:2831-2854.

16. Liu, J.Y., and Orville, H.D. (1969) Numerical modeling of precipitation and cloud shadow effects on mountain cumuli, J. Atmos. Sci. 26:1282-1298.

17. Mitchell, K. E. (1975) A Numerical Investigation of Severe Thunderstorm Gust Fronts, unpublished M.S. thesis, the Pennsylvania State University, 104 pp. (Also available from NTIS, No. N76-17737/7GI)

18. Schlesinger, R. E. (1973) A numerical model of deep moist convection: Part A prototype experiment and variations upon it, J. Atmos. Sci. 30:1374-1391.

19. Matthews, D. A. (1981) Observations of a cloud arc triggered by thunderstorm outflow, Mon. Wea. Rev. 109:2140-2157.